CONTINUOUS ADJOINT METHODS IN SHAPE, TOPOLOGY, FLOW-CONTROL AND ROBUST OPTIMIZATION

Open Source CFD International Conference, London 2012

Kyriakos C. Giannakoglou[1], Dimitrios I. Papadimitriou[1],
Evangelos M. Papoutsis-Kiachagias[1], Ioannis S. Kavvadias[1]
and Carsten Othmer[2]

[1]National Technical University of Athens,
School of Mechanical Engineering,
Lab. Of Thermal Turbomachines,
Parallel CFD & Optimization Unit
Zografou, Athens, 15710, Greece
e-mails: kgianna@central.ntua.gr, dpapadim@mail.ntua.gr,
vaggelisp@gmail.com, kavvadiasj@hotmail.com
[2]Volkswagen AG, CAE Methods, Group Research,
Letter Box 1777, D-38436 Wolfsburg, Germany
e-mail: carsten.othmer@volkswagen.de

Keywords: steady/unsteady adjoint, Hessian matrix computation, shape and topology optimization, optimal active flow control, robust design

Abstract: *Recent progress in the development of continuous adjoint methods for the computation of the first- and higher-order sensitivity derivatives of various objective functions in aero/hydrodynamics is presented. Regarding development of methods, this paper includes: (a) The continuous adjoint to low-Reynolds turbulence models by laying emphasis on the need to include the adjoint turbulence model equations into the optimization loop. (b) The continuous adjoint to turbulent flow solvers which use the wall function technique. (c) The truncated Newton method which relies on the computation of Hessian-vector products, as a more efficient alternative to the exact Newton method, in problems with many design variables. (d) The adjoint method for the solution of robust design problems, based on the second-order second-moment (SOSM) approach and a gradient-based algorithm, requiring the computation of up to third-order mixed derivatives w.r.t. the environmental and design variables. Regarding applications, the adjoint method is demonstrated in aero/hydrodynamic shape optimization problems, the optimization of steady/unsteady jet-based flow control systems and topology optimization problems in fluid mechanics. Steady and unsteady continuous adjoint methods are employed. Most of the methods presented in this paper have been implemented in OpenFOAM©, adding state of the art optimization capabilities to a widely used open source software.*

1 AERODYNAMIC OPTIMIZATION IN TURBULENT FLOWS

1.1 Flow Equations and Objective Functions

The system of state equations are presented in a way which covers shape, topology and flow control optimization problems. To do so, some extra terms depending on the porosity field α are appended to the Navier-Stokes equations. The new terms are useful only in topology optimization; otherwise, $\alpha \equiv 0$. The flow is incompressible and, without loss in generality, the Spalart-Allmaras turbulence model, [1], is used to effect closure in turbulent flows. Based on the above, the state equations are written as

$$R^p = 0, \quad R^{v_i} = 0, \quad R^T = 0, \quad R^{\widetilde{\nu}} = 0 \tag{1}$$

where

$$R^p = \frac{\partial v_j}{\partial x_j} \tag{2}$$

$$R^{v_i} = v_j \frac{\partial v_i}{\partial x_j} + \frac{\partial p}{\partial x_i} - \frac{\partial}{\partial x_j}\left[(\nu+\nu_t)\left(\frac{\partial v_i}{\partial x_j}+\frac{\partial v_j}{\partial x_i}\right)\right] + \alpha v_i \tag{3}$$

$$R^T = v_j \frac{\partial T}{\partial x_j} - \frac{\partial}{\partial x_j}\left[\left(\frac{\nu}{Pr}+\frac{\nu_t}{Pr_t}\right)\frac{\partial T}{\partial x_j}\right] + \alpha\left(T - T_{wall}\right) \tag{4}$$

$$R^{\widetilde{\nu}} = v_j \frac{\partial \widetilde{\nu}}{\partial x_j} - \frac{\partial}{\partial x_j}\left[\left(\nu+\frac{\widetilde{\nu}}{\sigma}\right)\frac{\partial \widetilde{\nu}}{\partial x_j}\right] - \frac{c_{b_2}}{\sigma}\left(\frac{\partial \widetilde{\nu}}{\partial x_j}\right)^2 - \widetilde{\nu}P\left(\widetilde{\nu}\right) + \widetilde{\nu}D\left(\widetilde{\nu}\right) + \alpha\widetilde{\nu} \tag{5}$$

The energy equation is optionally included in the system of state equations to account for flow problems with heat transfer. Here, v_i are the velocity components, p is the static pressure divided by the density, T is the static temperature, $\widetilde{\nu}$ is the turbulence state variable, ν is the bulk viscosity and ν_t is the turbulent viscosity given by $\nu_t = \widetilde{\nu}f_{v_1}$. Also, Pr, Pr_t are the laminar and turbulent Prandtl numbers and T_{wall} is the known-fixed temperature over the solidified parts of the domain in topology optimization problems with heat transfer. $R^{\widetilde{\nu}}$ must be ignored in laminar flows and so does R^T if heat transfer effects are not taken into consideration.

The applications presented in this paper are dealing with the following objective functions: (1) the volume-averaged total pressure losses between the inlet S_I and the outlet S_O of the domain Ω, (2) forces (for instance, lift, drag, etc) exerted on the solid walls S_W along a user-defined direction r_i, (3) the volume–averaged temperature difference between S_O and S_I, (4) the deviation of the hydraulic head H from a desirable value H_{tar} (for hydraulic turbomachines) and (5) the deviation of the pressure distribution p from a given distribution p_{tar} along S_w (inverse design problems). The corresponding five functions to

be minimized are defined below

$$F_1 = \int_{S_I} F_{S_I} dS + \int_{S_O} F_{S_O} dS = -\int_{S_I} \left(p + \frac{1}{2} v^2 \right) v_i n_i dS - \int_{S_O} \left(p + \frac{1}{2} v^2 \right) v_i n_i dS \quad (6)$$

$$F_2 = \int_{S_W} F_{S_W} dS = \int_{S_W} \left[-(\nu + \nu_t) \left(\frac{\partial v_i}{\partial x_j} + \frac{\partial v_j}{\partial x_i} \right) + p \, \delta_i^j \right] n_j r_i dS \quad (7)$$

$$F_3 = -\int_{S_I} T v_i n_i dS - \int_{S_O} T v_i n_i dS \quad (8)$$

$$F_4 = \frac{1}{2} (H - H_{tar})^2 \ , \ \ H = \frac{\int_{S_I} \left(p + \frac{1}{2} v_k^2 \right) v_i n_i dS + \int_{S_O} \left(p + \frac{1}{2} v_k^2 \right) v_i n_i dS}{g \int_{S_I} v_i n_i dS} \quad (9)$$

$$F_5 = \frac{1}{2} \int_{S_w} (p - p_{tar})^2 dS \quad (10)$$

where n_i is the outward unit normal vector and g the acceleration of gravity.

1.2 The Continuous Adjoint Method for Shape Optimization in Turbulent Flows

In turbulent flows, the development of continuous adjoint methods which take full account of the turbulence model PDEs is quite new in the literature. This is not the case in discrete adjoint, where the differentiation of the already discretized turbulence model equations is straightforward, [5, 6, 7]. In contrast, in continuous adjoint, the majority of the existing works use the "frozen turbulence" assumption, according to which the sensitivities of turbulence quantities w.r.t. the design variables b_m are neglected. The first work presenting the continuous adjoint to the Spalart-Allmaras turbulence model, for incompressible flows, is [2]. This was extended to compressible flows in [3]. Regarding the adjoint approach to high-Reynolds turbulence models, the continuous adjoint to the k-ε model with wall functions was firstly presented in [4]. This section presents briefly the underlying development and aims at convincing the reader that, in some cases, the solution of the adjoint turbulence model equation(s) is really necessary.

In shape optimization problems ($\alpha \equiv 0$), the total sensitivity derivatives (symbol δ) of any function Φ w.r.t. b_m are related to its partial sensitivities (symbol ∂) through the relation

$$\frac{\delta \Phi}{\delta b_m} = \frac{\partial \Phi}{\partial b_m} + \frac{\partial \Phi}{\partial x_l} \frac{\delta x_l}{\delta b_m} \quad (11)$$

where $\frac{\delta x_l}{\delta b_i}$ are the sensitivities of nodal coordinates. In topology or flow control optimization, where the grid is invariant, the last term vanishes. To develop the adjoint equations, the augmented objective function F_{aug} is defined by adding the field integrals of the products of the adjoint variable fields and the state equations to F, as follows

$$F_{aug} = F + \int_{\Omega} u_i R_i^v d\Omega + \int_{\Omega} q R^p d\Omega + \int_{\Omega} T_a R^T d\Omega + \int_{\Omega} \widetilde{\nu}_a R^{\widetilde{\nu}} d\Omega \quad (12)$$

Here, u_i are the adjoint velocity components, q is the adjoint pressure, T_a the adjoint temperature and $\widetilde{\nu}_a$ the adjoint to $\widetilde{\nu}$. The total variation (symbol δ) of F_{aug} w.r.t. b_m

reads

$$\frac{\delta F_{aug}}{\delta b_m} = \frac{\delta F}{\delta b_m} + \int_\Omega u_i \frac{\partial R_i^v}{\partial b_m} d\Omega + \int_\Omega q \frac{\partial R^p}{\partial b_m} d\Omega + \int_\Omega T_a \frac{\partial R^T}{\partial b_m} d\Omega + \int_\Omega \widetilde{\nu}_a \frac{\partial R^{\widetilde{\nu}}}{\partial b_m} d\Omega$$

$$+ \int_S u_i R_i^v \frac{\delta x_k}{\delta b_m} n_k dS + \int_S q R^p \frac{\delta x_k}{\delta b_m} n_k dS + \int_S T_a R^T \frac{\delta x_k}{\delta b_m} n_k dS$$

$$+ \int_S \widetilde{\nu}_a R^{\widetilde{\nu}} \frac{\delta x_k}{\delta b_m} n_k dS \tag{13}$$

where $S = S_I \cup S_O \cup S_w$ or (see [2] where all symbols are explained). After applying the Green-Gauss theorem, eq. 13 can be written as

$$\frac{\delta F_{aug}}{\delta b_m} = \int_\Omega R_i^u \frac{\partial v_i}{\partial b_m} d\Omega + \int_\Omega R^q \frac{\partial p}{\partial b_m} d\Omega + \int_\Omega R^{T_a} \frac{\partial T}{\partial b_m} d\Omega + \int_\Omega R^{\widetilde{\nu}_a} \frac{\partial \widetilde{\nu}}{\partial b_m} d\Omega$$

$$+ \int_S B_i^u \frac{\partial v_i}{\partial b_m} dS + \int_S B_{ij}^{Gu} \frac{\partial}{\partial b_m} \left(\frac{\partial v_i}{\partial x_j} \right) dS + \int_S B^q \frac{\partial p}{\partial b_m} dS + \int_S B^{T_a} \frac{\partial T}{\partial b_m} dS$$

$$+ \int_S B_i^{GT} \frac{\partial}{\partial b_m} \left(\frac{\partial T}{\partial x_i} \right) dS + \int_S B^{\widetilde{\nu}_a} \frac{\partial \widetilde{\nu}}{\partial b_m} dS \int_S B_i^{G\widetilde{\nu}_a} \frac{\partial}{\partial b_m} \left(\frac{\partial \widetilde{\nu}}{\partial x_i} \right) dS + SD \tag{14}$$

The last term, SD, is a sum of integrals (see eq. 19) which depend only on the sensitivities of geometrical quantities and leads to the expression of sensitivity derivatives of F. The elimination of all field (Ω) integrals depending on the sensitivities of the flow variables $(\frac{\partial v_i}{\partial b_m}$, etc.) from eq. 14 gives rise to the following adjoint mean flow and turbulence model equations

$$R^q = \frac{\partial u_j}{\partial x_j} = 0 \tag{15}$$

$$R^{u_i} = -v_j \left(\frac{\partial u_i}{\partial x_j} + \frac{\partial u_j}{\partial x_i} \right) + \frac{\partial q}{\partial x_i} - \frac{\partial}{\partial x_j} \left[(\nu + \nu_t) \left(\frac{\partial u_i}{\partial x_j} + \frac{\partial u_j}{\partial x_i} \right) \right]$$

$$- \widetilde{\nu} \frac{\partial \widetilde{\nu}_a}{\partial x_i} - \frac{\partial}{\partial x_k} \left(e_{jki} e_{jmq} \frac{\mathcal{C}_S(\widetilde{\nu})}{S} \frac{\partial v_q}{\partial x_m} \widetilde{\nu} \widetilde{\nu}_a \right) - T \frac{\partial T_a}{\partial x_i} + \alpha u_i = 0 \tag{16}$$

$$R^{T_a} = -v_j \frac{\partial T_a}{\partial x_j} - \frac{\partial}{\partial x_j} \left[\left(\frac{\nu}{Pr} + \frac{\nu_t}{Pr_t} \right) \frac{\partial T_a}{\partial x_j} \right] + \alpha T_a = 0 \tag{17}$$

$$R^{\widetilde{\nu}_a} = -v_j \frac{\partial \widetilde{\nu}_a}{\partial x_j} - \frac{\partial}{\partial x_j} \left[\left(\nu + \frac{\widetilde{\nu}}{\sigma} \right) \frac{\partial \widetilde{\nu}_a}{\partial x_j} \right] + \frac{1}{\sigma} \frac{\partial \widetilde{\nu}_a}{\partial x_j} \frac{\partial \widetilde{\nu}}{\partial x_j} + 2 \frac{c_{b2}}{\sigma} \frac{\partial}{\partial x_j} \left(\widetilde{\nu}_a \frac{\partial \widetilde{\nu}}{\partial x_j} \right) + (D - P) \widetilde{\nu}_a$$

$$+ \widetilde{\nu}_a \widetilde{\nu} \, \mathcal{C}_{\widetilde{\nu}}(\widetilde{\nu}, \vec{v}) + \frac{\delta \nu_t}{\delta \widetilde{\nu}} \frac{\partial u_i}{\partial x_j} \left(\frac{\partial v_i}{\partial x_j} + \frac{\partial v_j}{\partial x_i} \right) + \frac{\delta \nu_t}{\delta \widetilde{\nu}} \frac{1}{Pr_t} \frac{\partial T_a}{\partial x_j} \frac{\partial T}{\partial x_j} + \alpha \widetilde{\nu}_a = 0 \tag{18}$$

where, in shape optimization, $\alpha \equiv 0$. The elimination of the boundary integrals that depend on the sensitivities of the flow variables from eq. 14 yields the adjoint boundary conditions, as exposed in detail in [2]. The remaining terms, which have been abbreviated to SD, define the sensitivity derivatives of F w.r.t. b_m, namely

$$\frac{\delta F}{\delta b_m} = \int_{S_W} \frac{\partial F_{S_W}}{\partial x_k} \frac{\delta x_k}{\delta b_m} dS + \int_{S_W} F_{S_W} \frac{\delta(dS)}{\delta b_m} - \int_{S_W} \left[\nu \left(\frac{\partial u_i}{\partial x_j} + \frac{\partial u_j}{\partial x_i} \right) n_j - q n_i \right] \frac{\partial v_i}{\partial x_k} \frac{\delta x_k}{\delta b_m} dS$$

$$+ \int_{S_W} u_i R_i^v \frac{\delta x_k}{\delta b_m} n_k dS + \int_{S_W} q R^p \frac{\delta x_k}{\delta b_m} n_k dS + \int_{S_W} \nu \frac{\partial F_{S_W}}{\partial p} \frac{\partial}{\partial x_k} \left(\frac{\partial v_i}{\partial x_j} + \frac{\partial v_j}{\partial x_i} \right) \frac{\delta x_k}{\delta b_m} n_i n_j dS$$

$$+ \int_{S_W} \nu \frac{\partial F_{S_W}}{\partial p} \left(\frac{\partial v_i}{\partial x_j} + \frac{\partial v_j}{\partial x_i} \right) \frac{\delta(n_i n_j)}{\delta b_m} dS - \int_{S_W} \nu \frac{\partial \widetilde{\nu}_a}{\partial x_j} n_j \frac{\partial \widetilde{\nu}}{\partial x_k} \frac{\delta x_k}{\delta b_m} dS + \int_\Omega \widetilde{\nu}_a \widetilde{\nu} \mathcal{C}_\Delta(\widetilde{\nu}, \vec{v}) \frac{\partial \Delta}{\partial b_m} d\Omega \tag{19}$$

where $\mathcal{C}_S(\widetilde{\nu})$, $\mathcal{C}_{\widetilde{\nu}}(\widetilde{\nu},\vec{v})$ and $\mathcal{C}_\Delta(\widetilde{\nu},\vec{v})$ result from the Spalart–Allmaras model equations. Terms such as $\frac{\delta x_k}{\delta b_m}$, $\frac{\delta(dS)}{\delta b_m}$, $\frac{\delta(n_i n_j)}{\delta b_m}$, etc. depend on the selected parameterization scheme for the shape (S_w) to be designed and can be computed either numerically or analytically.

The shape optimization of an elbow duct for min. $F = F_1$, (eq. 6), is shown in fig. (1) In this figure, the computed sensitivity derivatives $\frac{\delta F}{\delta b_m}$ are shown on the left, where b_m stand for the normal displacements of the solid wall grid nodes. Two sensitivity distributions are presented and compared (a) by solving the complete adjoint system, including the adjoint to the Spalart-Allmaras PDEs (marked as "turbulent adjoint") and (b) by making the "frozen turbulence" assumption. The abscissa stands for the IDs of the inner wall nodes. It is clear that, by making the "frozen turbulence" assumption, wrongly signed sensitivities are computed for nodes with ID from 20 to 50. The duct shape along with the velocity isolines are shown on the right of fig. (1). This is a convincing example showing that the omission of solving the adjoint turbulence model equation(s) (i.e. the omission of solving eq. 18) may mislead the optimization by computing derivatives $\frac{\delta F}{\delta b_m}$ with the wrong sign.
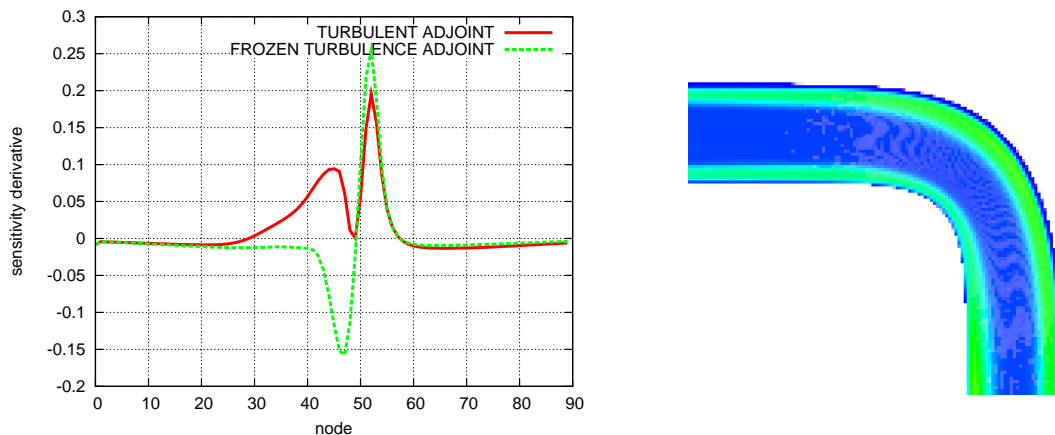

Figure 1: Shape optimization of an elbow duct for min. total pressure losses. Results from [2].

The previous development was based on the low-Reynolds number Spalart-Allmaras model. However, several engineering applications still rely on (high-Reynolds number) turbulence models with wall functions, since their use allows handling coarser grids and saving CPU cost. For this reason, in [4], the continuous adjoint approach to the high-Reynolds $k-\varepsilon$ turbulence model, was presented for incompressible flows. In [4], the concept of the *adjoint wall functions* was introduced for the first time in the corresponding literature. The adjoint friction velocity was introduced to bridge the gap between the wall boundary faces and the first cell-centres off the wall, during the solution of the adjoint equations.

The concept presented in [4] (there, employed to an in-house, vertex-centered flow solver based on the pseudo-compressibility technique) was, then, adapted to the high-Reynolds variant of the Spalart-Allmaras method in OpenFOAM©. In the latter, a single law of the wall expression is used to model the inner sublayer and the logarithmic part of the turbulent boundary layer, [8],

$$f_{WF} = y^+ - v^+ - e^{-\kappa B}\left[e^{\kappa v^+} - 1 - \kappa v^+ - \frac{(\kappa v^+)^2}{2} - \frac{(\kappa v^+)^3}{6}\right] = 0 \qquad (20)$$

where $\kappa = 0.41$, $B \approx 5.5$ and the non-dimensional distance and velocity are $y^+ = \frac{y v_\tau}{\nu}$ and

$v^+ = \frac{|v_i|_P}{v_\tau}$ Also, v_τ is the (primal or state) friction velocity, computed by

$$v_\tau^2 = \left[(\nu + \nu_t) \left(\frac{\partial v_i}{\partial x_j} + \frac{\partial v_j}{\partial x_i} \right) \right]_f n_j t_i \tag{21}$$

where n_j and t_i are, the normal and tangent to the wall unit vectors. Subscripts f and P denote quantities defined at the boundary wall face and the first cell centre, respectively (see fig. 2). The computation of $\left. \frac{\partial v_i}{\partial x_j} \right|_f n_j$, eq. 21, using any finite-difference scheme intro-
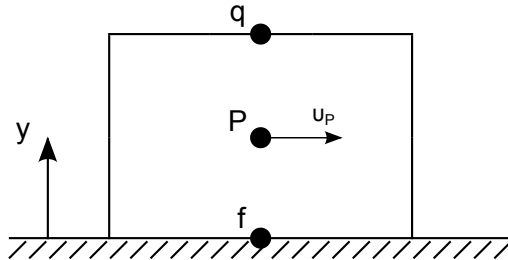
Figure 2: Typical finite volume adjacent to the wall.

duces error. This is alleviated by computing an "artificial" value of $\nu_t|_f$, so that the wall shear stress computed by eq. 20 and that computed by differentiating the velocity field and multiplying by $(\nu + \nu_t)_f$ be identical. So, $f_{WF}(v_\tau, |v_i|_P, y_P) = 0$ (eq. 20) is solved for v_τ and then, eq. 21 adjusts $\nu_t|_f$ accordingly.

According to the development presented in [4] for a different turbulence model, the adjoint friction velocity, $u_\tau^2 = \left[(\nu + \nu_t) \left(\frac{\partial u_i}{\partial x_j} + \frac{\partial u_j}{\partial x_i} \right) \right]_f n_j t_i$, is introduced in order to correctly compute the adjoint viscous fluxes at f. The rest of the adjoint formulation previously developed for its low–Reynolds counterpart is adapted accordingly.

An indicative application is presented in fig. (3), where the gain in accuracy is illustrated. A non-symmetric NACA4415 airfoil was parameterized using Bézier polynomials with 8 control points for the pressure and suction sides, fig. (3)–top. A hybrid grid was used with a mean $y^+ \approx 10$ for all nodes P (fig. 2) along the solid walls. The Reynolds number is $Re = 6 \times 10^6$ based on the airfoil chord length and the infinite flow angle is $\alpha_\infty = 3^o$. The state equations include the Spalart-Allmaras model with wall functions, as programmed in OpenFOAM©.

The proposed method for calculating sensitivity derivatives using the adjoint wall functions technique was used to calculate the sensitivities of $F = F_2$ (eq. 7) with respect to the (x, y) coordinates of the 16 control points, resulting to a total of 32 design variables (including the leading and trailing edge control points). The outcome of this calculation ("adjoint WF") is compared with finite differences ("FD") in fig. (3)–bottom left. The two curves are in a very good agreement even for the leading and trailing edge control points, where the "usual" flow singularities often lead to local inaccuracies. In fig. (3)–bottom right, the two aforementioned curves are also compared with those computed using the "frozen turbulence" assumption and the adjoint to the low–Reynolds Spalart-Allmaras model. The latter implies that the primal solver uses the Spalart–Allmaras model with wall functions but the adjoint is based on its low–Reynolds variant. The gain in accuracy is obvious and it is interesting to note that, in this case, the "low–Reynolds" approach performs even worse than the "frozen turbulence assumption"!
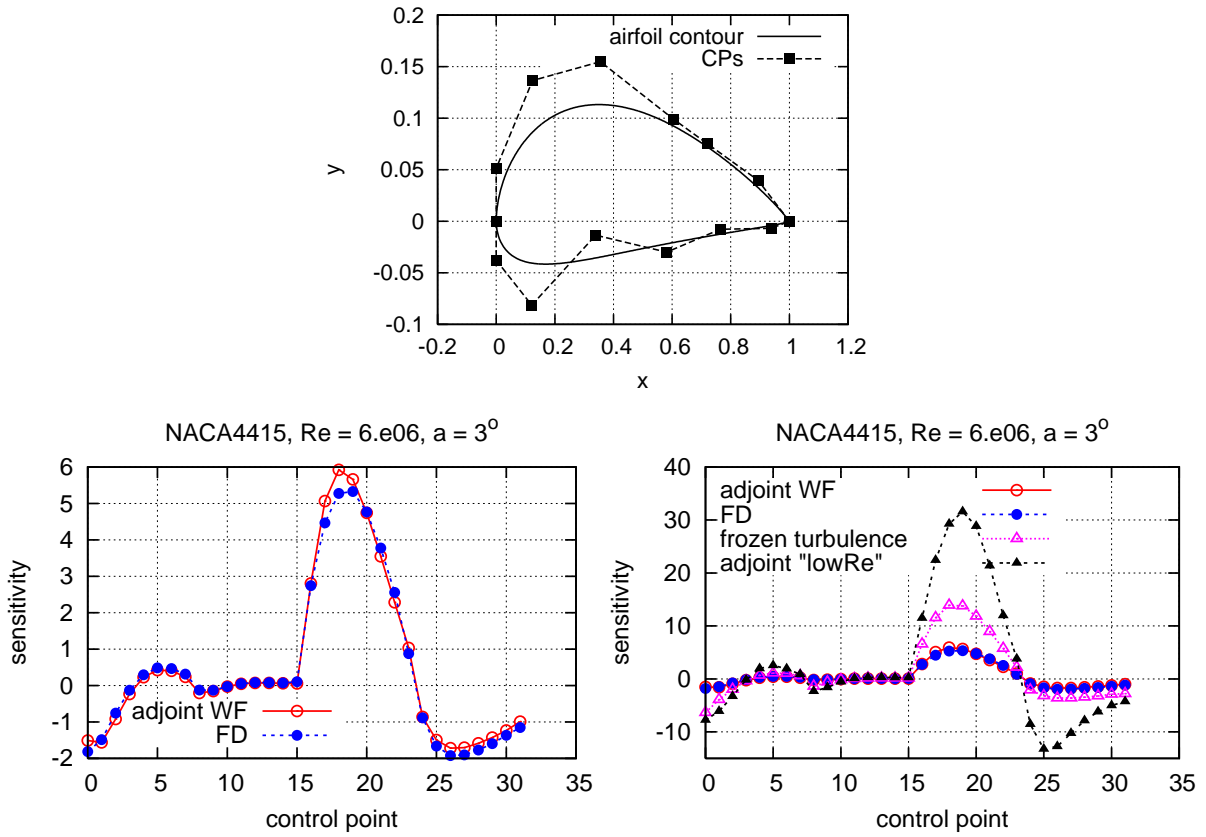
Figure 3: Shape optimization of the NACA4415 airfoil for min. $F = F_2$, (eq. 7). Coordinates x and y (top) are not in scale.

In fig. 4, the application of the presented adjoint approaches to two industrial problems is presented. The first case (top) is concerned with the design of a Francis turbine runner for the desired target head H_{tar} (min. F_4, eq. 9), subject to a number of flow constraints. Pressure distributions over the initial (left) and optimal (right) runners are shown in the figure. The second case (bottom) is concerned with the shape optimization of the Volkswagen L1 concept car, targeting minimum drag force (min. F_2, eq. 7), [12]. The rear part of the car is parameterized by drawing morphing boxes (left) and the comparative view of the baseline and the optimized geometries, with the corresponding sensitivity derivatives, is also presented (right).
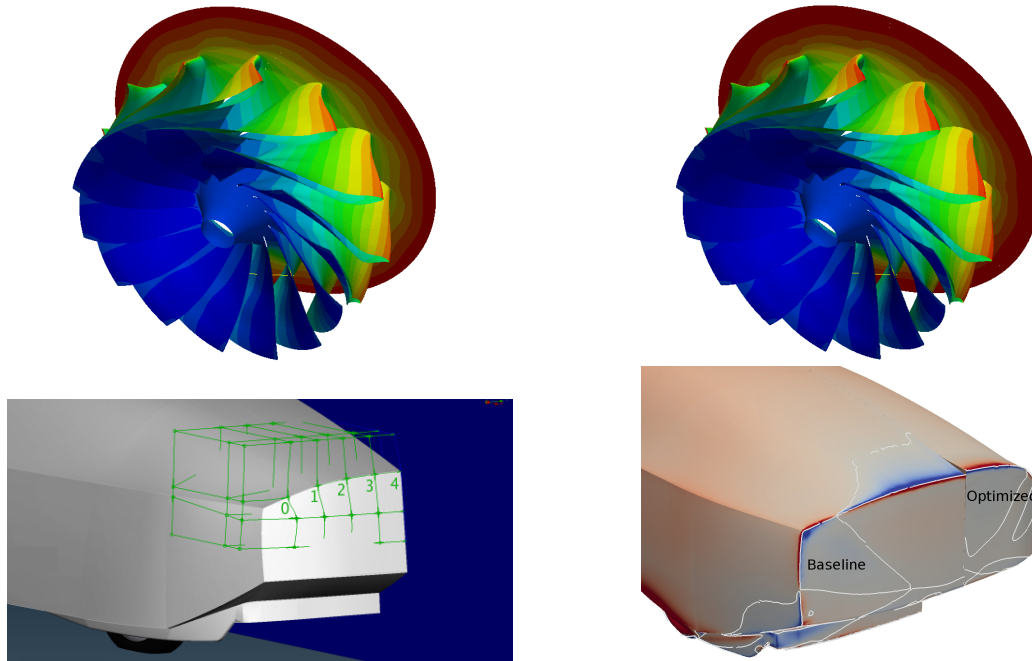
Figure 4: Top: Optimization of a Francis runner blade for increased hydraulic head. Bottom: Optimization of the VW L1 concept car targeting minimum drag force, [12].

1.3   Adjoint for Optimal Flow Control (Steady Jet)

The continuous adjoint method is used as a tool to identify the appropriate location and "type" (suction or blowing) of steady jets used in active flow control systems. It computes sensitivity maps along S_w, from which the designer extracts information about the optimal location (from the sensitivity magnitude) and "type" (from the sensitivity sign) of the jet to be applied, so as to successfully control the boundary layer development.

In such a problem, the design variables are the values of the Cartesian components of hypothetical jet velocities v_{pq}^b ($p \in [1, 2]$ in $2D$ or $p \in [1, 3]$ in $3D$ problems) at the N wall boundary nodes ($q \in [1, N]$). Since $\frac{\delta x_k}{\delta b_i} = 0$, it can be proved that, for any objective function F, at any point over S_w, the sensitivity derivatives are

$$\frac{1}{\Delta S_q} \frac{\delta F}{\delta v_{pq}^b} = (\nu + \nu_t) \left(\frac{\partial u_{pq}}{\partial x_j} + \frac{\partial u_{jq}}{\partial x_p} \right) n_{jq} - q_q n_{pq} \tag{22}$$

Eq. 22 has been derived for $F = F_1$, (eq. 6) without including the energy equation $R^T = 0$ into the system of flow PDEs. Without loss in generality, it is assumed that the jet velocities v_{jet} are normal to the wall. Thus, the signed jet velocities v_{jet} become $v_q^{jet} = v_{pq}^b n_{pq}^b$ (summation over p) and their sensitivity derivatives $\frac{\delta F}{\delta v_q^{jet}} = \frac{\delta F}{\delta v_{pq}^b} n_{pq}^b$. High absolute valued sensitivities pinpoint the most promising locations for the placement of jets. The sensitivity sign at these points indicates the preferred direction of the jet, i.e. suction or blowing (negative and positive sign, respectively). Such a case is illustrated in fig. 5 where the flow control in an S–shaped duct for min. $F = F_1$ is examined. In this figure, the distribution of nodal sensitivity derivatives $\frac{1}{\Delta S} \frac{\delta F}{\delta v_q^{jet}}$ along the lower and upper walls is plotted. The sensitivities computed using the continuous adjoint method (labeled "Adjoint") perfectly match those computed using finite differences ("FD"). This figure shows

the recommended jet locations. On the right, the computed velocity magnitude isolines are presented. With two suction slots, having max. jet velocities equal to 10% of the inlet flow velocity, applied at the recommended locations (kinks in the sensitivity map), a reduction in viscous losses, from 0.01835 to 0.01432 was achieved.
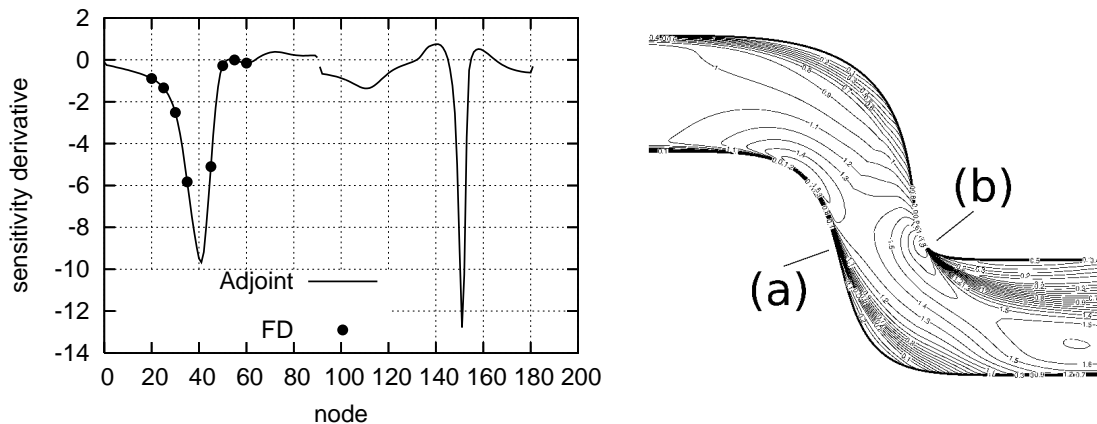

Figure 5: Flow control using steady blowing or suction jets, in an S–shaped duct for min. total pressure losses.

1.4 Adjoint for Optimal Flow Control (Unsteady Jet)

A similar application using unsteady (pulsating, either for blowing of for suction) jets, which requires the use of unsteady adjoint methods follows. The distribution of jets alongside the body is fixed and the design variables will be the amplitudes of all jet velocities. This problem calls for solving the unsteady primal equations and the unsteady adjoint equations. The only differences with respect to the adjoint equations, eqs. (15-18), are the extra temporal terms.

In order to solve the adjoint equations backwards in time, the checkpointing method with the binomial distribution for optimal memory-space usage [21, 22] is used.

The adjoint method was used to support steepest descent, for calculating the optimal amplitude of each jet, in order to minimize the time-averaged drag of the square cylinder shown in fig. (6). The jet velocities at the predefined slots, as shown in fig. (6), are given by

$$v_i^b = (A^b \sin(2\pi f^b t + f_0^b) - A^b)n_i , \quad i = 1, 2(3) \tag{23}$$

where the frequency f and phase f_0 are fixed ($f = \frac{U_\infty}{D} = 10, f_0 = 0$), while the amplitudes A^b stand for the design variables. The pulsating jet period is not to be confused with the period of the free flow unsteadiness, which is associated with the Strouhal number of the flow. The flow is laminar and the Reynolds number is $Re = 100$, which causes von-Karman vortices to be generated behind the body. The Strouhal number was calculated $St = 0.145$. At the end of the optimization, the mean drag coefficient was significantly reduced (fig. (6)-top), which was in fact the optimization target. The minimization of lift was not implemented in the objective function, but lift was zeroed thanks to the pulsating jet, and this was a by-product of the optimization. In the same figure, bottom, the computed optimal jets are shown and their amplitudes are tabulated. The infinite velocity magnitude was $U_{inf} = 0.1\frac{m}{s}$. Snapshots of the flow vorticity in the controlled case, over a jet-period of time T_{jet}, is presented in fig. (7).

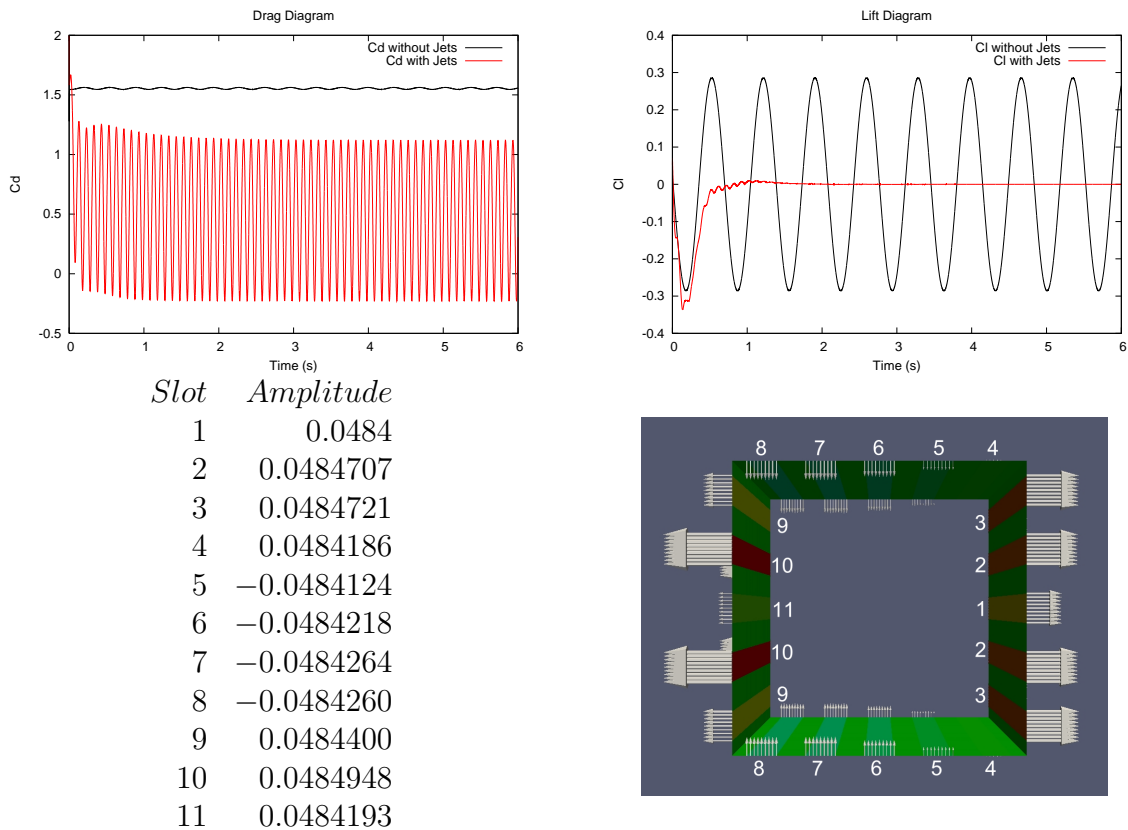| Slot	Amplitude
1	0.0484
2	0.0484707
3	0.0484721
4	0.0484186
5	−0.0484124
6	−0.0484218
7	−0.0484264
8	−0.0484260
9	0.0484400
10	0.0484948
11	0.0484193

Figure 6: Mean Drag Minimization for an unsteady laminar flow around a square cylinder, using pulsating jets. Optimization assisted by the unsteady continuous adjoint method. A similar study for a circular cylinder, using discrete adjoint however, can be found in [20].

1.5   Topology Optimization using Continuous Adjoint

In fluid mechanics, topology optimization is a useful tool for designing flow passages which connect given inlets and outlets and yield optimal performance according to an objective function F. The continuous adjoint method for the solution of topology optimization problems in incompressible flows, with or without heat transfer, was presented in [9],[10] and [11]. Constraints on the volume flow rates and mean temperatures per outlet boundary are optionally imposed.

To formulate the topology optimization problem, a real-valued porosity field α is artificially introduced into the governing equations (see eqs. 2). The porosity field α that minimizes F is sought. Upon convergence of the optimization method, the local porosity values identify the domain areas that correspond to the flowing fluid (nodes with $\alpha = 0$ or, practically, $\alpha \leq \varepsilon$ where $\varepsilon > 0$ is an infinitesimally small quantity). For $\alpha = 0$, eqs. 2 to 5 degenerate to the conventional flow equations. All the remaining areas with $\alpha \neq 0$ or, practically $\alpha > \varepsilon$, correspond to parts of the domain to be solidified, [11]. There, according to eqs. 2 to 5, $v_i = 0, T = T_{wall}, \widetilde{\nu} = \nu_t = 0$. Interfaces between fluid and solid are thus computed, which correspond to the optimal solid walls. For this type of problems, the adjoint method is the right choice because the cost for computing the gradient of F is independent of the number of design variables which coincides with the grid size. The adjoint equations are given by eqs. 15 to 18.

(a) $t = T_{jet}$

(b) $t = T_{jet} + \frac{1}{5}T_{jet}$

(c) $t = T_{jet} + \frac{2}{5}T_{jet}$

(d) $t = T_{jet} + \frac{3}{5}T_{jet}$

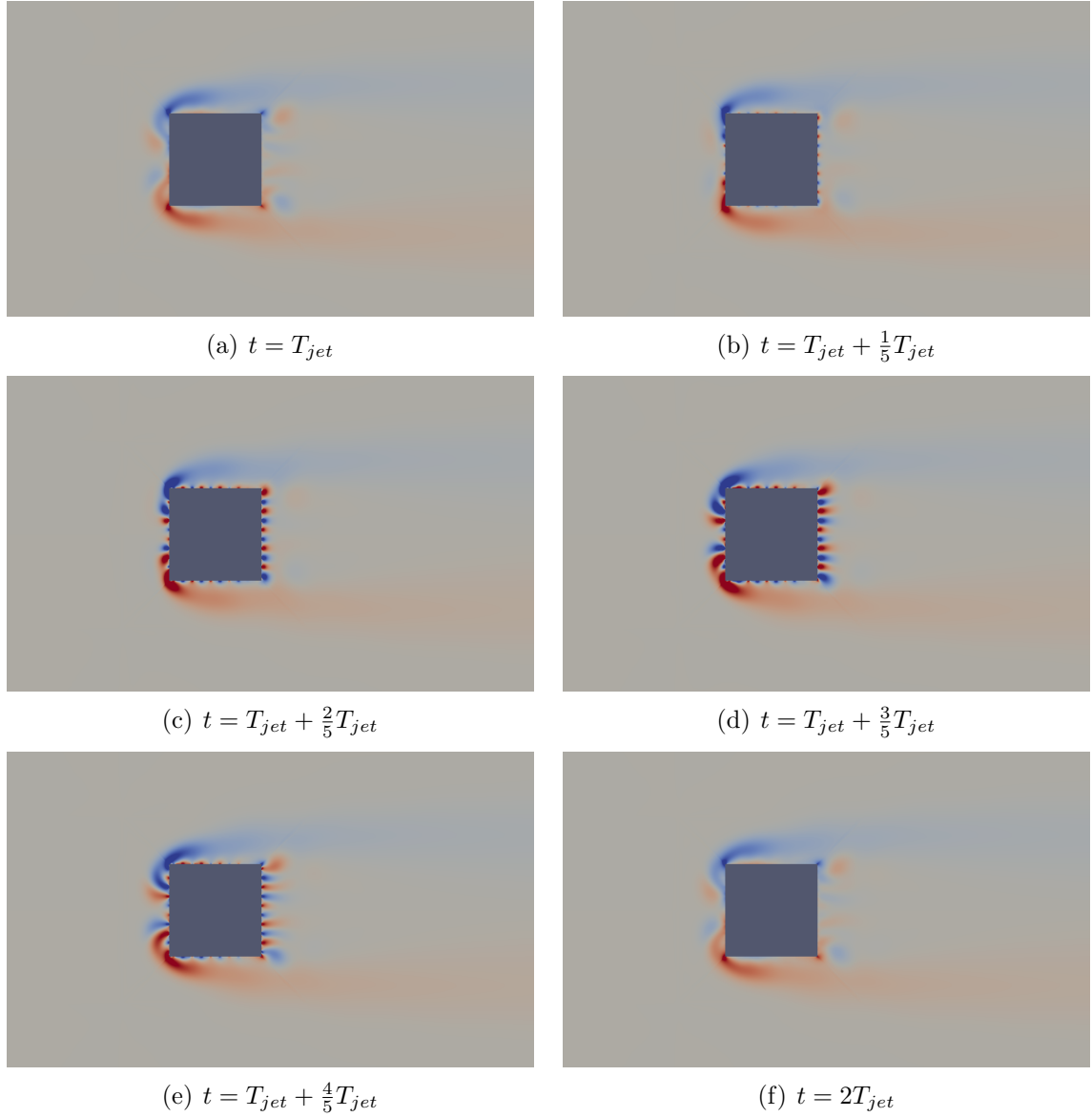(e) $t = T_{jet} + \frac{4}{5}T_{jet}$

(f) $t = 2T_{jet}$

Figure 7: Mean Drag Minimization for an unsteady laminar flow around a square cylinder, using pulsating jets: Vorticity field snapshots equi-distributed over a jet-period T_{jet}.

In the first case presented below, the objective function considered is the weighted sum of the total pressure losses (min. F_1, eq. 6) and the temperature difference (min. F_3, eq. 8). Thus, $F = w_1 F_1 - w_3 F_3$, where w_1 and w_3 are user–defined weights, should be minimized. With this objective function, the sensitivity derivative w.r.t. α at the k–th grid cell is given by the expression

$$\frac{\delta F_{aug}}{\delta \alpha_k} = (v_i u_i \Omega)_k + [(T - T_{wall})T_a \Omega]_k + [\widetilde{\nu}\widetilde{\nu}_a \Omega]_k + \int_\Omega \widetilde{\nu}_a \widetilde{\nu} \mathcal{C}_\Delta(\widetilde{\nu}, \vec{v}) \frac{\partial \Delta}{\partial \alpha_k} d\Omega \qquad (24)$$

where Ω_k is the finite volume of cell k, associated with α_k. The flow is considered to be turbulent and the Spalart-Allmaras turbulent model is used.

For the above-mentioned objective function, optimal solutions to two topology optimization problems including flow constraints are illustrated in fig. 8. On the left, the constrained topology optimization of a one-inlet/four-outlet duct, aiming at min. $F = F_1$

11

$(w_1 = 1, w_2 = 0)$ and requiring 25% of the incoming flow rate to exit from each outlet is presented while, on the right, the topology optimization of the same duct subject to the constraint of equal mean temperatures at all outlets and targeting min. $F = F_1 - 0.01F_3$ $(w_1 = 1, w_2 = 0.01)$ can be seen. Velocity iso-areas (left) and flow trajectories along with the imposed T_{wall} distribution (right) are shown.
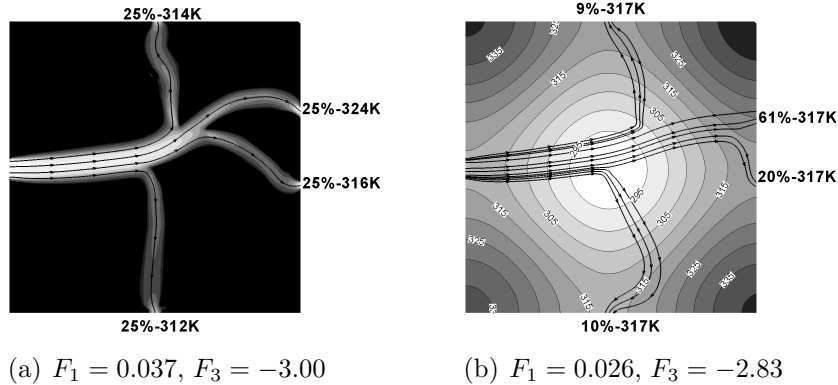

(a) $F_1 = 0.037, F_3 = -3.00$ (b) $F_1 = 0.026, F_3 = -2.83$

Figure 8: Topology optimization targeting min. total pressure losses and an equally distributed flow mass between the four outlets (left). Minimization of $F = F_1 - 0.01F_3$ along with the constraint of temperature uniformity at the four outlets (right). From [10].

An industrial application of topology optimization is presented in fig. (9). The target is to minimize $F = F_1$ for an air-conditioning duct of a commercial passenger car. In the top-left figure, the duct geometry is presented along with the description of the duct boundaries. In top-right, the flow trajectories of the initial duct's solution can be seen. In bottom-left, the final porosity field is presented and the corresponding flow trajectories can be seen, bottom-right. The optimization of the duct, using topology optimization, leads to a 42% reduction in total pressure losses.
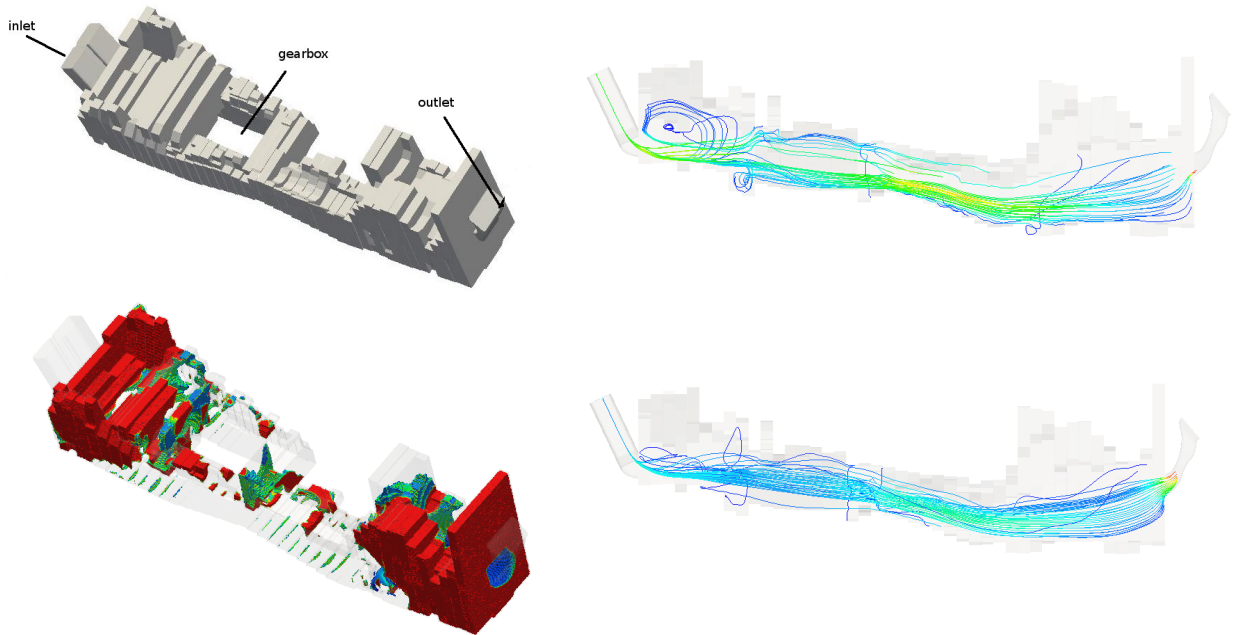
Figure 9: Topology optimization of an air-conditioning duct targeting min. $F = F_1$. Test case from the E.C. project "Flowhead".

2 COMPUTATION AND USE OF HIGHER-ORDER SENSITIVITY DERIVATIVES

All previous sections were concerned with the computation of first-order sensitivity derivatives and their application in shape, topology and flow control optimization using gradient-based methods such as steepest descent or, even, quasi-Newton variants. However, gradient-based optimization algorithms suffer from convergence degradation, especially in problems where there are different scales in the gradient components.

A remedy to this problem is to solve the Newton equation

$$\frac{\delta^2 F}{\delta b_i \delta b_j}\bigg|^k \delta b_j = -\frac{\delta F}{\delta b_i}\bigg|^k, \qquad b_j^{k+1} = b_j^k + \delta b_j \tag{25}$$

for updating the design variables, instead of using steepest-descent or a quasi-Newton method such as BFGS. The Newton method requires the (Hessian) matrix of second-order sensitivity derivatives $\frac{\delta^2 F}{\delta b_i \delta b_j}$ (in addition to the gradient, $\frac{\delta F}{\delta b_i}$) in order eq. 25 to be solved for δb_j. The computation of the Hessian of F can be carried out in four different ways, which can be set up in either discrete or continuous form, [13, 14, 15]. These four ways rely on all possible combinations of the direct differentiation (DD) and the adjoint variable (AV) method. They noticeably differ in terms of computing cost. The latter is measured in terms of equivalent flow solutions (EFS). One EFS stands for the CPU cost of numerically solving the flow equations, i.e. the state or primal problem.

The most efficient approach to compute the Hessian matrix is the so-called DD-AV method which is based on DD to compute the first-order derivatives of F and the adjoint approach to compute the second-order ones. The overall computing cost is equal to $N + 1$ EFS, excluding the cost for solving the state equations.

The alternative approach AV-DD, where the first-order sensitivities are computed using the adjoint approach and the second-order ones by differentiating the adjoint equa-

tions, is less efficient and requires as many as $2N + 1$ EFS. However, as shown in section 2.1, the AV-DD approach is the most efficient approach for the computation of Hessian-vector products needed for the truncated Newton algorithm. This method fits well to very large scale problems, such as the computation of sensitivity maps for complex shapes or in topology optimization, where the design variables are as many as the grid cells of nodes. In either case, there might be thousands or millions of design variables.

In the sake of completeness, the DD-DD approach is the most costly one, since its cost scales with N^2. On the other hand, it can be shown that the AV-AV approach can be transformed to either DD-AV or AV-DD.

If there is a moderate number of design variables or the Hessian matrix itself has to be computed (this might be useful for the computation of the objective function in robust design problems, see below, even in the framework of a global optimization method), the DD-AV approach is the most efficient one. Since, in the so-called truncated Newton method, the solution of eq. 25 is required, rather than the computation of the Hessian matrix itself, the AV-DD approach can preferably be used. Similar developments with exactly the same costs in EFS hold for the discrete approach, [15]. Below, the truncated Newton method, as applied to topology (rather than shape) optimization, [17], is briefly presented. The implementation of truncated Newton in shape optimization can be found in [16].

2.1   The Truncated Newton Method in Topology Optimization

The truncated Newton method is based on the use of the Conjugate Gradient (CG) method with M_{CG} cycles for the solution of linear systems, where M_{CG} is usually much smaller than the number of design variables. The CG algorithm solves iteratively linear systems, such as $A_{mn}x_n = q_m, (m,n) \in [1, N]$. Starting from the initialization $x^\rho = x^0$ ($\rho = 0$) and the corresponding residuals $r_m^0 = A_{mn}x_n^0 - q_m^0$ and $s_m^0 = -r_m^0$, the following steps:

$$
\begin{aligned}
w_m &= A_{nm}s_n, \quad m \in [1, N] \\
\eta &= \frac{r_m^\rho r_m^\rho}{s_m w_m} \\
x_m^{\rho+1} &= x_m^\rho + \eta s_m, \quad m \in [1, N] \\
r_m^{\rho+1} &= r_m^\rho + \eta w_m, \quad m \in [1, N] \\
\beta &= \frac{r_m^{\rho+1} r_m^{\rho+1}}{r_m^\rho r_m^\rho} \\
s_m &= -r_m^{\rho+1} + \beta s_m, \quad m \in [1, N]
\end{aligned}
\tag{26}
$$

are performed ($\rho \leftarrow \rho+1$; ρ is the CG cycle counter) until the norm of the new residual $r^{\rho+1}$ is lower than a user-defined threshold value. The cost of each CG cycle, comprising the previous six steps, is practically nothing more than the cost of performing the matrix-vector multiplication in the first step. In topology optimization, the Newton equation, eq. 25 to be solved, is similar to the aforementioned linear system, if $A_{mn} = \frac{\delta^2 F}{\delta \alpha_m \delta \alpha_n}$ and $q_m = -\frac{\delta F}{\delta \alpha_m}$.

For instance, in topology optimization for laminar flows, aiming at minimum total pressure losses, the sensitivities of the objective function are given by the expression, [10],

$$
\frac{\delta F}{\delta \alpha_m} = u_i^m v_i^m \Omega_m
\tag{27}
$$

where m indicates the cell index and u_i satisfy the adjoint equations given in the previous section. Eq. 27 is a simplified version of eq. 24, for laminar flows without heat transfer.

The Hessian vector products required by the truncated Newton method are computed using the expression

$$
\begin{aligned}
\frac{\delta^2 F}{\delta\alpha_m \delta\alpha_n}s_n &= \int_\Omega \left(v_i \frac{\delta u_i}{\delta\alpha_n}s_n + u_i\frac{\delta v_i}{\delta\alpha_n}s_n \right)\frac{\delta\alpha}{\delta\alpha_m}d\Omega = \int_\Omega \left(v_i\bar{u}_i + u_i\bar{v}_i \right)\frac{\delta\alpha}{\delta\alpha_m}d\Omega \\
&= \left(v_i^m\bar{u}_i^m + u_i^m\bar{v}_i^m \right)\Omega_m
\end{aligned}
\tag{28}
$$

where fields $\frac{\delta v_i}{\delta\alpha_n}s_n = \bar{v}_i$ and $\frac{\delta u_i}{\delta\alpha_n}s_n = \bar{u}_i$ are computed from the differentiation of the flow and adjoint equations w.r.t. α and their multiplication with s, yielding

$$
\frac{\partial\bar{v}_j}{\partial x_j}=0
$$

$$
\bar{v}_j\frac{\partial v_i}{\partial x_j} + v_j\frac{\partial\bar{v}_i}{\partial x_j} + \frac{\partial\bar{p}}{\partial x_i} - \frac{\partial}{\partial x_j}\left[\nu\left(\frac{\partial\bar{v}_i}{\partial x_j}+\frac{\partial\bar{v}_j}{\partial x_i}\right)\right] + \alpha\bar{v}_i + sv_i=0\ , \qquad i=1,2 \tag{29}
$$

and

$$
\frac{\partial\bar{u}_j}{\partial x_j}=0
$$

$$
-\bar{v}_j\left(\frac{\partial u_i}{\partial x_j}+\frac{\partial u_j}{\partial x_i}\right) - v_j\left(\frac{\partial\bar{u}_i}{\partial x_j}+\frac{\partial\bar{u}_j}{\partial x_i}\right) - \nu\frac{\partial}{\partial x_j}
$$

$$
\left(\frac{\partial\bar{u}_i}{\partial x_j}+\frac{\partial\bar{u}_j}{\partial x_i}\right) + \frac{\partial\bar{q}}{\partial x_i} + \alpha\bar{u}_i + su_i = 0, \quad i=1,2 \tag{30}
$$

respectively. The boundary conditions for systems 29 and 30 are derived from the differentiation of the flow and adjoint boundary conditions w.r.t. α_n and their multiplication with s_n.

The adjoint-based truncated Newton method for topology optimization is demonstrated in the case of a square overall domain which has two flow inlets and two outlets and three square "obstacles" inside. The optimal velocity distribution computed using the truncated Newton, in an one-shot fashion, is shown in fig. 10, left. The objective function value converges in an almost 4% lower value when using the truncated Newton algorithm instead of the steepest descent one, fig. 10, right.

2.2   Solution of Robust Shape Optimization Problems

Robust design methods in aerodynamics aim at optimizing a shape in a range of operating conditions or by considering the effect of environmental uncertainties, such as manufacturing imprecisions, fluctuations of flow conditions, etc. All uncertainties depend on the so-called environmental variables $\mathbf{c}\,(c_i, i \in [1, M])$. In robust design problems, the function to be minimized can be expressed as $\widehat{F}=\widehat{F}\,(\mathbf{b}, \mathbf{c}, \mathbf{U}(\mathbf{b}, \mathbf{c}))$, to denote the dependency of $\widehat{F}$ on both $\mathbf{U}$, the design variables $\mathbf{b}\,(b_l, l \in [1, N])$ which parameterize the aerodynamic shape and the environmental variables $\mathbf{c}\,(c_i, i \in [1, M])$. The adjoint method (AV), coupled with DD, can also be used to solve robust design problems using any gradient–based method. According to the Second-Order Second-Moment (SOSM) approach, a probability density function $g(\mathbf{c})$ is associated with $\mathbf{c}$ and the function $\widehat{F}$ to be minimized depends
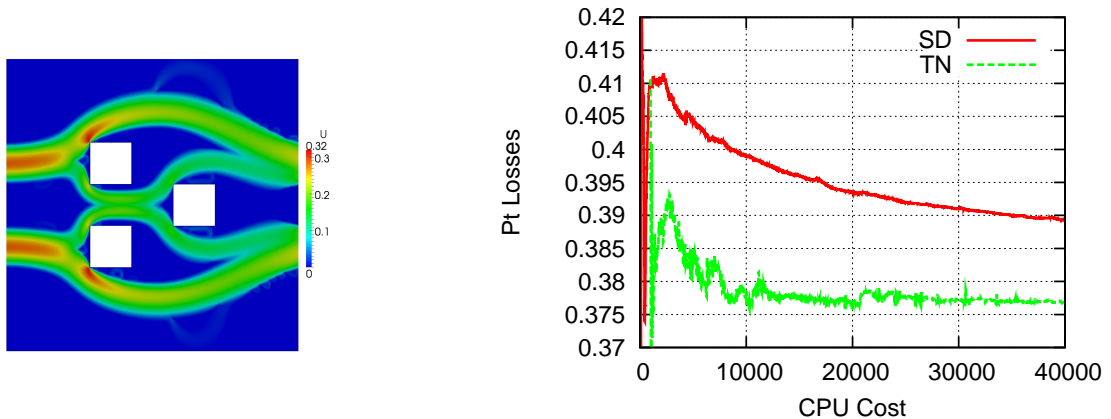
Figure 10: Topology optimization of a duct with three obstacles. Gain from using the truncated Newton method. From [17].

on the mean value μ_F and the variance $\sigma_F{}^2$ of F. These are defined as

$$\mu_F(\mathbf{b}, \mathbf{c}) \;=\; \int F g(\mathbf{c}) d\mathbf{c} \simeq F + \frac{1}{2}\left[\frac{\delta^2 F}{\delta c_i^2}\right]_{\overline{\mathbf{c}}} \sigma_i^2 \tag{31}$$

$$\sigma_F{}^2(\mathbf{b}, \mathbf{c}) \;=\; \int (F - \mu_F)^2 g(\mathbf{c}) d\mathbf{c} \simeq \left[\frac{\delta F}{\delta c_i}\right]_{\overline{\mathbf{c}}}^2 \sigma_i^2 + \frac{1}{2}\left[\frac{\delta^2 F}{\delta c_i \delta c_j}\right]_{\overline{\mathbf{c}}}^2 \sigma_i^2 \sigma_j^2 \tag{32}$$

where the gradients are evaluated at the mean values $\overline{\mathbf{c}}$ of the environmental variables.

In robust design, the function $\widehat{F}$ to be minimized becomes

$$\widehat{F}(\mathbf{b}, \mathbf{c}) = w_1 \mu_F + w_2 \sigma_F^2 \tag{33}$$

where w_1 and w_2 are user-defined weights. It is evident that, even for computing the value of $\widehat{F}$, first- and second-order derivatives of F w.r.t. $\mathbf{c}$ are required. Therefore, even, if the optimization problem is to be solved using a stochastic method (such as evolutionary algorithms), the methods presented in this paper are needed to compute μ_F and $\sigma_F{}^2$. If a gradient-based method is selected to solve the problem, the gradient of $\widehat{F}$ w.r.t. the design variables b_q must be available. By differentiating eq. 33 w.r.t. b_q, this becomes, [18],

$$\frac{\delta \widehat{F}}{\delta b_q} = w_1 \left(\frac{\delta F}{\delta b_q} + \frac{1}{2}\frac{\delta^3 F}{\delta c_i^2 \delta b_q}\sigma_i^2\right) + w_2 \frac{2\frac{\delta F}{\delta c_i}\frac{\delta^2 F}{\delta c_i \delta b_q}\sigma_i^2 + \frac{\delta^2 F}{\delta c_i \delta c_j}\frac{\delta^3 F}{\delta c_i \delta c_j \delta b_q}\sigma_i^2 \sigma_j^2}{2\sqrt{\left[\frac{\delta F}{\delta c_i}\right]^2 \sigma_i^2 + \frac{1}{2}\left[\frac{\delta^2 F}{\delta c_i \delta c_j}\right]^2 \sigma_i^2 \sigma_j^2}} \tag{34}$$

From eq. 34, $\frac{\delta \widehat{F}}{\delta b_q}$ requires the computation of up to third-order mixed sensitivities w.r.t. c_i and b_q, such as $\frac{\delta^3 F}{\delta c_i \delta c_j \delta b_q}$. These computations are presented in detail in [18, 19].

The DD_c-DD_c-AV_b is the most efficient method to solve the problem with a gradient-based method provided that the number of environmental variables (M) is smaller than the number of design variables (N). DD_c mean that direct differentiation is performed w.r.t. $\mathbf{c}$ whereas in AV_b the adjoint method undertakes the derivation w.r.t. $\mathbf{b}$. It is reasonable to reserve the use of the adjoint method for the array (this is $\mathbf{b}$ in our case) with the higher dimension. So, all $\frac{\delta F}{\delta b_q}$ derivatives are computed using the AV method, at the cost of a single EFS. First- and second- order derivative w.r.t. $\mathbf{c}$ ($\frac{\delta F}{\delta c_i}$ and $\frac{\delta^2 F}{\delta c_i \delta c_j}$) rely

on DD. This means that $\frac{\delta U}{\delta c_i}$ and $\frac{\delta^2 U}{\delta c_i \delta c_j}$ (where U stands for the flow or state variables) will be computed at the cost of M and $\frac{M(M+1)}{2}$ EFS, respectively. Once $\frac{\delta U}{\delta c_i}$ and $\frac{\delta^2 U}{\delta c_i \delta c_j}$ have been computed, the computation of $\frac{\delta F}{\delta c_i}$ and $\frac{\delta^2 F}{\delta c_i \delta c_j}$ is straightforward. Regarding the computation of derivatives $\frac{\delta^2 F}{\delta c_i \delta b_q}$ and $\frac{\delta^3 F}{\delta c_i \delta c_j \delta b_q}$, the previously computed first or second order derivatives of F w.r.t. **c** should be differentiated w.r.t. to **b**. As in the standard continuous adjoint method, to compute $\frac{\delta^2 F}{\delta c_i \delta b_q}$, a new augmented objective function must be defined in which, in addition to the state equations, their derivatives with respect to **c** must be also added. This development introduces M new adjoint variable fields for which M PDEs must be numerically solved at the cost of M EFS. Similarly, for $\frac{\delta^3 F}{\delta c_i \delta c_j \delta b_q}$, a new augmented objective function will also include the Hessian of the state equations. The corresponding development introduces $\frac{M(M+1)}{2}$ EFS. By also including the cost of solving the state equations, the computation of $\frac{\delta \hat{F}}{\delta b_q}$, eq. 34, has an overal cost of

$$1 + 1 + M + M + \frac{M(M+1)}{2} + \frac{M(M+1)}{2} = 2 + 3M + M^2 \ EFS$$

EFS. In [19], this is presented using both the discrete and continuous approaches and an interesting comparison of the two formulations is shown.

Fig. (11) presents the use of the aforementioned method for the robust inverse design of a 2D symmetric cascade. On the left, a comparison of sensitivities $\frac{\delta \mu_F}{\delta b_q}$ (b_q are the coordinates of Bézier control points) computed using the proposed method (DD$_c$-DD$_c$-AV$_b$) and finite differences (FD) is shown. On the right, the convergence of the mean value and standard deviation of F using $w_1 = 0.7, w_2 = 0.3$ is presented, [19].
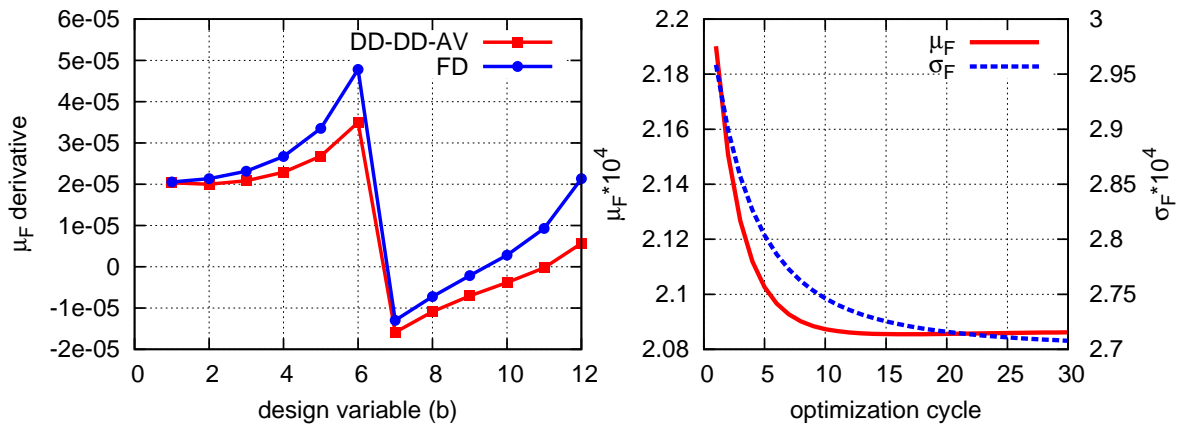

Figure 11: Robust inverse design of a 2D symmetric cascade (min. $F = F_6$, eq. 10). From [19].

Acknowledgments

References

[1] Spalart P, Allmaras S. (1992) A one-equation turbulence model for aerodynamic flows. *AIAA Paper*, 92-0439; 1992

[2] A.S. Zymaris, D.I. Papadimitriou, K.C. Giannakoglou, C. Othmer: Continuous adjoint approach to the Spalart-Allmaras turbulence model for incompressible flows, *Computers & Fluids*, 38 (2009), 1528–1538.

[3] A. Bueno-Orovio, C. Castro, F. Palacios, E. Zuazua: Continuous Adjoint Approach for the SpalartAllmaras Model in Aerodynamic Optimization *AIAA Journal*, 50 (2012), 631–646.

[4] A.S. Zymaris, D.I. Papadimitriou, K.C. Giannakoglou, C. Othmer: Adjoint wall functions: A new concept for use in aerodynamic shape optimization, *Journal of Computational Physics*, 229 (2010), 5228–5245.

[5] C.S. Kim, C. Kim, O.H. Rho: Feasibility study of constant eddy–viscosity assumption in gradient–based design optimization. *Journal of Aircraft*, 40(2003), 1168-1176.

[6] B.J. Lee, C. Kim: Automated design methodology of turbulent internal flow using discrete adjoint formulation. *Aerospace Science and Technology*, 11 (2007), 163-173.

[7] D.J. Mavriplis: Discrete adjoint–based approach for optimization problems on three–dimensional unstructured meshes. *AIAA Journal*, 45 (2007), 740-750.

[8] N.T. Frink: Assessment of an Unstructured-Grid Method for Predicting 3-D Turbulent Viscous Flows. *AIAA Paper* 96-0292, 1996.

[9] E.M. Papoutsis-Kiachagias, E.A. Kontoleontos, A.S. Zymaris, D.I. Papadimitriou, K.C. Giannakoglou: Constrained topology optimization for laminar and turbulent flows, including heat transfer. *EUROGEN Conference 2011*, Capua, Italy.

[10] E.A. Kontoleontos, E.M. Papoutsis-Kiachagias, A.S. Zymaris, D.I. Papadimitriou, K.C. Giannakoglou: Adjoint-based constrained topology optimization for viscous flows, including heat transfer. *Engineering Optimization*, DOI:10.1080/0305215X.2012.717074, 2012.

[11] Othmer C.: A continuous adjoint formulation for the computation of topological and surface sensitivities of ducted flows, *International Journal for Numerical Methods in Fluids*, 58(2008), 861-877.

[12] C. Othmer, E. Papoutsis-Kiachagias, K. Haliskos: CFD Optimization via Sensitivity-Based Shape Morphing. *4th ANSA & μETA International Conference*, Thessaloniki, Greece, 2011.

[13] D.I. Papadimitriou, K.C. Giannakoglou: Computation of the Hessian matrix in aerodynamic inverse design using continuous adjoint formulations. *Computers & Fluids*, 37 (2008), 1029–1039.

[14] D.I. Papadimitriou, K.C. Giannakoglou: The continuous direct-adjoint approach for second-order sensitivities in viscous aerodynamic inverse design problems, *Computers & Fluids*, 38 (2008), 1539–1548.

[15] D.I. Papadimitriou, K.C. Giannakoglou: Aerodynamic shape optimization using adjoint and direct approaches, *Archives of Computational Methods in Engineering*, 15 (2008), 447–488.

[16] D.I. Papadimitriou, K.C. Giannakoglou: Aerodynamic Design using the Truncated Newton Algorithm and the Continuous Adjoint Approach. *International Journal for Numerical Methods in Fluids*, 68 (2012), 724-739.

[17] D.I. Papadimitriou, E.M. Papoutsis-Kiachagias, K.C. Giannakoglou: Topology Optimization in Fluid Dynamics using Adjoint-Based Truncated Newton. *ECCOMAS CFD 2012*, Vienna, Austria, 2012.

[18] E.M. Papoutsis-Kiachagias, D.I. Papadimitriou, K.C. Giannakoglou: Robust design in aerodynamics using third-order sensitivity analysis based on discrete adjoint. Application to quasi-1D flows. *International Journal for Numerical Methods in Fluids*, 69 (2012), 691-709.

[19] E.M. Papoutsis-Kiachagias, D.I. Papadimitriou, K.C. Giannakoglou: On the optimal use of adjoint methods in aerodynamic robust design problems. *CFD and OPTI-MIZATION 2011, ECCOMAS Thematic Conference*, Antalya, Turkey, 2011.

[20] Carnarius A., Thiele F., Özkaya E., Nemili A., Gauger N.R. (2012). Optimal Control of Unsteady Flows Using Discrete Adjoints. *AIAA paper* 2011-3720, 2011.

[21] A. Griewank, A. Walther: Algorithm 799: revolve: an implementation of checkpointing for the reverse or adjoint mode of computational differentiation. *Transactions on Mathematical Software* 26 (1), 19-45 (2000)

[22] Wang, Q., (2008). Uncertainty Quantification for Unsteady Fluid Flow Using Adjoint-Based Approaches *Phd Thesis*, Standford University, USA.